

Lab on a Chip

Accepted Manuscript



This is an *Accepted Manuscript*, which has been through the Royal Society of Chemistry peer review process and has been accepted for publication.

Accepted Manuscripts are published online shortly after acceptance, before technical editing, formatting and proof reading. Using this free service, authors can make their results available to the community, in citable form, before we publish the edited article. We will replace this *Accepted Manuscript* with the edited and formatted *Advance Article* as soon as it is available.

You can find more information about *Accepted Manuscripts* in the [Information for Authors](#).

Please note that technical editing may introduce minor changes to the text and/or graphics, which may alter content. The journal's standard [Terms & Conditions](#) and the [Ethical guidelines](#) still apply. In no event shall the Royal Society of Chemistry be held responsible for any errors or omissions in this *Accepted Manuscript* or any consequences arising from the use of any information it contains.

Cite this: DOI: 10.1039/c0xx00000x

www.rsc.org/xxxxxx

ARTICLE TYPE

Microfluidic fabrication of cell-derived nanovesicles as endogenous RNA carriers

Wonju Jo,^a Dayeong Jeong,^b Junho Kim,^b Siwoo Cho,^a Su Chul Jang,^c Chungmin Han,^a Ji Yoon Kang,^d Yong Song Gho^{†*c} and Jaesung Park^{†*ab}

⁵ Received (in XXX, XXX) Xth XXXXXXXXX 20XX, Accepted Xth XXXXXXXXX 20XX
DOI: 10.1039/b000000x

Exosomes /microvesicles are known to shuttle biological signals between cells, possibly by transferring biological signal components such as encapsulated RNAs and proteins, plasma membrane proteins, or both. Therefore exosomes are being considered for use as RNA and protein delivery vehicles for various therapeutic applications. However, living cells in nature secrete only a small number of exosomes, and procedures to collect them are complex; these complications impede their use in mass delivery of components to targeted cells. We propose a novel and efficient method that forces cells through hydrophilic microchannels to generate artificial nanovesicles. These mimetic nanovesicles contain mRNAs, intracellular proteins and plasma membrane proteins, and are shaped like cell-secreted exosomes. When recipient cells are exposed to nanovesicles from embryonic stem cells, mRNAs of Oct 3/4 and Nanog are transferred from embryonic stem cells to the target cells. This result suggests that mimetic nanovesicles can be used as vehicles to deliver RNA. This nanovesicle formation method is expected to be used in exosome research and to have applications in drug and RNA-delivery systems.

Introduction

Exosomes /microvesicles secreted from cells have been subjects of intensive research recently. These cell-secreted exosomes are nano-scale compartments with an enclosed lipid bilayer membrane that can deliver biological components between cells¹⁻⁵. Due both to surface membrane proteins on the lipid bilayer membrane and the exosomes' nano-scale diameter, the trans-membrane delivery abilities of cell-secreted exosomes allow for easy endocytosis⁶⁻¹⁰. Since they are found to be involved in intercellular communications as natural RNA-delivery vehicles, intensive efforts have been made to exploit these abilities for targeted RNA-delivery¹¹.

Although RNA-delivery systems show promise for therapeutic applications in several diseases (e.g. genetic disorders, diabetes, cancer), several hurdles must be overcome before one can be used for therapeutic purposes¹²⁻¹⁶. One major hurdle is to deliver RNA across the plasma membrane with high efficiency and low toxicity. Conventional RNA-delivery techniques include

electroporation and viral vector injection, but they have drawbacks in efficiency and safety due to their immunogenicity and cellular toxicity^{9, 17-19}. Recent efforts to improve the delivery systems include use of polymers, microfluidics, lipoproteins and lipid-like particles (lipidoids); these approaches have been reported to have better efficiency and safer characteristics than the conventional ones²⁰⁻²³. For similar purposes, efforts have been made to develop drug and RNA delivery systems that use small liposomes, which have a lipid bilayer membrane²⁴⁻²⁸. Recently, immiscible flow microfluidic channels using a micronozzle or flow focusing techniques in microchannels have been tried without the lyophilization process²⁶⁻³⁰. Nevertheless, these liposomes described above lack membrane proteins which have important functions during endocytosis, and may require several processes to tether specific molecules on the membranes³¹⁻³³. In contrast to these methods, when origin cells which secrete exosomes are either transfected with a short-hairpin-RNA coding vector, or loaded with small interfering RNA through an electroporated plasma membrane, the exosomes from origin cells have membrane proteins, and can be used as delivery vehicles for RNA interference (RNAi)^{34, 35}.

In this study, we demonstrate endogenous RNA-delivery using exosomes-mimetic nanovesicles. The nanovesicles are fabricated using living cells and microchannels to fabricate nano-scale vesicles. The lipid membrane in the fabricated nanovesicles is derived from living embryonic stem cell (ES cell) membranes, and contains intact membrane proteins. We discovered that the fabricated nanovesicles contained the same RNAs as the cytoplasm and also proved that these nanovesicles can deliver

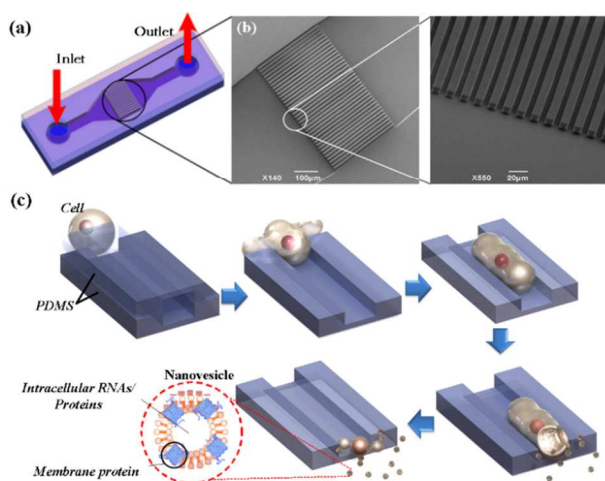
^aDept. Mechanical Engineering, POSTECH, San 31, Hyoja-dong, Nam-gu, Pohang, Gyeongbuk, Republic of Korea. Fax: +82-54-279-5899; Tel: +82-54-279-5418; E-mail: jpark@postech.ac.kr

^bSchool of Interdisciplinary Bioscience and Bioengineering, POSTECH, San 31, Hyoja-dong, Nam-gu, Pohang, Gyeongbuk, Republic of Korea. Fax: 82-54-279-5899; Tel: 82-54-279-2188; E-mail: jpark@postech.ac.kr

^cDepartment of Life Science, Pohang University of Science and Technology San 31, Hyoja-dong, Namgu, Pohang, Gyeongbuk, Republic of Korea; E-mail: ysgcho@postech.ac.kr

^dCenter for Biomicrosystem, Korea Institute of Science and Technology (KIST), Seoul, Republic of Korea

[†] These authors are co-corresponding authors.



loaded

Figure 1. (a) Cell suspension was pressurized through parallel microchannels through which cells flow. (b) SEM images of the 37 microchannels in parallel (c) Schematic process of nanovesicle generation. As cells flow through slits in microchannels, cells are stretched. At the outlet of the microchannels, nanovesicles are generated possibly due to abrupt pressure change and elongated shape caused by shear stress.

intracellular RNAs into the cytoplasm of targeted cells. These results suggest that the fabricated nanovesicles are similar to exosomes, and are effective for delivery of loaded contents, e.g. RNAs.

Materials and Methods

Microchannel fabrication

The microchannel was patterned using soft lithography in SU-8 2025 with a thickness of 10 μm (Figure 1a, b). Channels were fabricated (a) with a constant length of 200 μm and a width of 3, 5, or 7 μm or (b) with a constant width of 5 μm and a length of 100, 200, or 400 μm . For each case, the number of microchannels was 37 in parallel. These SU-8 patterns were used as the masters for microchannels made of nine parts polydimethylsiloxane (PDMS) silicon elastomer base and one part curing agent. PDMS microchannels treated with oxygen plasma were then bonded to glass and baked for 2 h at 150 $^{\circ}\text{C}$ to create a tight bond. The microchannels on the bonded devices were treated with the plasma, then the devices then stored for 24 h in phosphate buffer saline (PBS) to preserve their hydrophilic property. To test the effect of surface hydrophobicity during nanovesicle generation, a hydrophobic micro-channel was made separately using 2% PTFE (Dupont Teflon[®] AF: Amorphous Fluoropolymer solution) in a solvent (ACROS FC-75).

Cell culture

The murine embryonic stem (ES) cell line-D3 (ATCC, CRL-1934) was used as a source of nanovesicles. The cells were cultured in knockout DMEM (Gibco), supplemented with 15 % replacement fetal bovine serum (Gibco), 4 mM L-glutamine (Sigma), 100 g/mL penicillin-streptomycin (Gibco), 1000 U/mL leukemia inhibitory factor (Chemicon, Temecula, CA), and 0.1

mM 2-Mercaptoethanol (Sigma) on a 150-mm culture dish coated with 0.1 % gelatin solution. The culture medium was replaced every day and cells were passaged with 1:10 dilution ratio at least once a week. Cells from passage numbers 4-18 were used for the experiments. The cells were cultured at 37 $^{\circ}\text{C}$ in a 95 % air / 5 % CO₂ atmosphere.

NIH-3T3 fibroblasts (ATCC, CRL-1658) were cultured in DMEM (Gibco), and supplemented with 10 % fetal bovine serum (Gibco) on a 150-mm culture dish. The culture medium was replaced every two days and cells were passaged at 1:10 dilution ratio when the dishes containing cells were 90 % full. The cells were cultured at 37 $^{\circ}\text{C}$ in a 90 % air / 10 % CO₂ atmosphere.

Nanovesicle generation and separation

An acrylic vise was fabricated and assembled with the microchannels to prevent leakage of samples during extrusion. During extrusion, the syringe pump was placed on a shaker to prevent cells from settling in the syringe. When ES cells had almost filled the culture dish, but had not formed an embryonic body, they were detached with 2 mM EDTA (Gibco) and suspended (1.5×10^6 cells/mL) in PBS and 0.5 mM ethylenediaminetetraacetate and then loaded in a 1 mL disposable syringe. They were then extruded through the fabricated microchannels using a syringe pump (11 plus dual syringe, Harvard Apparatus, USA). As a pre-cleaning process, extruded samples were collected and centrifuged at 1×10^3 g for 20 min to eliminate unbroken cells. Next, following the similar separation procedures for exosome³⁶, the supernatants were put into cushions consisting of 10% or 50% Optiprep solutions, which were then centrifuged at 1×10^5 g for 2 h. The centrifuged sample had several layers; the nanovesicles were in the second layer from the bottom, which was collected. All nanovesicle generation processes except the cell preparation were conducted at 4 $^{\circ}\text{C}$ to maintain the materials below the phase transition temperature of the lipid membrane to prevent cell aggregation and retain the solid-like state of plasma membranes during the processes.

Exosome preparation

When culture dishes containing ES cells were 80~90 % full, the culture medium was changed to a serum-free-medium containing DMEM (Gibco) supplemented with 4 mM L-glutamine (Sigma), 100 U/mL penicillin-streptomycin (Gibco), 1000 U/mL leukemia inhibitory factor (Chemicon, Temecula, CA), and 0.1 mM 2-mercaptoethanol (Sigma). After 24 h, the culture media was collected and centrifuged at 800 g for 5 min, then at 3000 g for 20 min to remove the remaining cells. Microparticles were also removed using a high speed centrifuge at 10,000 g for 30 min. Next, the supernatant was concentrated on a 50-kDa cutoff-membrane in a centrifuge tube (Amicon, Witten, Germant) at 1300 g to a volume of 10 mL. The concentrated sample was collected and centrifuged at 1×10^5 g for 2 h. Vesicles secreted from cells accumulated on the bottom of the tube after centrifuging.

Quantification of nanovesicles and exosomes

The collected nanovesicles were quantified using Bradford protein assay. In this quantification, the surface proteins are for quantifying indirectly the amount of surface proteins tethered on the surface of nanovesicles and exosomes³⁶⁻³⁸

Dynamic light scattering

The size and zeta potentials of the nanovesicles were measured using a dynamic laser scattering (DLS) instrument (Zetasizer 3000HSA, Malvern Instrument). 1 mL of nanovesicles was quantified with Bradford protein assay as described above, and prepared with a concentration of 5 µg/mL for measurement.

Transmission electron microscopy

The morphologies of exosomes and nanovesicles were observed by transmission electron microscopy (TEM, Joel 10011, Japan). The sample was prepared with a concentration of 50 µg/mL, which was quantified based on the surface proteins on nanovesicles with Bradford protein assay as described above. Samples (5 µL) were loaded on the grid and incubated for 3 min at room temperature. The sample on the edge of the grid was removed using filter paper and 5 µL uranyl acetate was loaded on the grid surface. The remaining uranyl acetate was removed using filter paper and the sample was dried. Then, the sample was observed using TEM.

RNA isolation

RNA preparation was conducted using Qiazol (Qiagen) according to the manufacturer's instructions. The RNA concentration of nanovesicles was measured using Nano-drop (Nano-Drop Technologies, Wilmington, DE, USA). The quality and size of RNA were examined on an Agilent RNA 6000 Nano Chip with a 2100 Bioanalyzer™ (Agilent Technologies, Santa Clara, CA).

Reverse transcription-polymerase chain reaction

To confirm the existence of RNA in nanovesicles and to compare it with origin cells, the reverse transcription-polymerase chain reaction (PCR) was conducted. These reactions were initiated using 100 ng RNA and 0.02 µM oligo dT to attach dT to the end of the RNA at 70 °C for 5 min, and the sample was stored at 4 °C for 5 min. The reverse transcription reaction was carried out at 42 °C for 70 min and 70 °C for 15 min. The actin, Oct 3/4 and Nanog sequences were amplified by PCR with the following primers to yield 200 bp, 100 bp and 400 bp product, respectively. PCR was performed in tubes containing 2 µL of the extracted cDNA and 23 µL of a master mixture. The PCR conditions consisted of denaturation at 94°C for 2 min, followed by 32 cycles of amplification at 94°C for 30 s, 56°C for 30 s, 72°C for 1 min and extension at 70°C for 5 min. PCR products were analysed by running samples on a 1% agarose gel for 30 min at 100 mV. The gel was stained with ethidium bromide for 10 min and was photographed with the BioDoc-It imaging system (UVP, Cambridge, UK).

The mouse Actin, Oct3/4 and Nanog primers used for PCR:

Actin	Forward	ACGTTGACATCCGTAAGAC
	Reverse	GACGTAATCTCCTTCTGCAT
Oct 3/4	Forward	AGACCATGTTTCTGAAGTGC
	Reverse	GAACCATACTCGAACCACAT
Nanog	Forward	AGGGTCTGCTACTGAGATGCTCTG
	Reverse	CAACCACTGGTTTTTCTGCCACCG

Western blotting

Protein preparation was conducted using RIPA buffer (Bio-Rad) according to the manufacturer's instructions. Equal amounts (10 g) of samples were separated by electrophoresis on a 8% SDS-PAGE gel and proteins were then transferred onto PVDF membranes. The membranes were blocked with 3% non-fat milk in phosphate buffered saline (PBS) for 1 h at room temperature and incubated with primary antibodies in 3% non-fat milk at 4°C overnight. After they were washed using 0.05% Tween-20 in PBS, they were incubated with secondary antibodies in 3% non-fat milk at room temperature for 1 h. The membranes were washed again and immunoreactive bands were visualized with a chemi-luminescent substrate. The following primary and secondary antibodies were used: Anti-actin (Santa cruz, sc-81178), Anti-ICAM-1 (Santa cruz, sc-1506), Anti-Nanog (Millipore, AB9220), Anti-mouse HRP (Santa cruz, sc-2096), Anti-goat HRP (Santa cruz, sc-2020) and Anti-rabbit HRP (Santa cruz, sc-2004). Primary antibodies were diluted 1:2000 and secondary antibodies were diluted 1:4000.

Flow cytometry

ES cells were dyed using CellTrace™ CFSE proliferation kit (Molecular Probes, C34554) then extruded to generate dyed nanovesicles. They were treated to NIH-3T3 fibroblasts with a concentration of 10 µg/mL. The treatment times for the nanovesicles were 0, 1 h, and 12 h. Treated NIH-3T3 fibroblasts were cultured at 37 °C in a 90 % air / 10 % CO₂ atmosphere. After 12 h, the cells in each well were detached using 250 µL Tryp-LE (Gibco). The detached cells were collected in a FACS tube with 1 mL DMEM + 10 % fetal bovine serum medium. The uptake rate of nanovesicles by NIH-3T3 fibroblasts was measured by FACS (Gallios, Beckman Coulter) using fluorescent intensity.

Confocal microscopy

ES cells were dyed using CellTracker™ Orange CMTMR (Molecular Probes, C2927) were extruded to generate dyed nanovesicles. 4×10⁴ NIH-3T3 fibroblast-GFP (Cell Biolabs, AKR-214) were placed on a confocal dish (SPL, 10035) with 0.2% gelatin (Sigma, G6144). The treatment times for the nanovesicles were 1h, and 12 h. They were washed in PBS and fixed using 4% paraformaldehyde. Nuclei were dyed using Hoechst (Sigma, B2883). Samples were treated with mounting solution (Invitrogen, 008010) to prevent dehydration. The samples were observed using confocal microscopy (Carl Zeiss, LSM 510 Meta).

Result and Discussion

Nanovesicle formation

Amphiphiles in aqueous solution self-assemble to reduce their thermodynamic energy by forming certain structures: topologically, micelles or bilayers; and geometrically, spheres, cylinders or planes. Many studies have investigated the factors that affect self-assembled structures, including temperature, properties of acyl chains, and head groups of the lipid molecule³⁹. Assuming that aggregated amphiphiles all have the same chemical potential, the equation describing thermodynamic equilibrium on self-assembly is

$$X_N = NX_i^N \exp[N(\mu_i^0 - \mu_N^0)/(kT)] \quad (1)$$

where N is the number of amphiphiles incorporated in the aggregated form, X_N is mole fraction of aggregated amphiphiles with aggregation number N , μ_N^0 is the molecules' self-free energy (J) with aggregation number N , k is Boltzmann's constant (J/K) and T is temperature (K)³⁹. Superscript 0 of μ_N^0 denotes that this free energy is the standard molecular interaction energy without entropy term. μ_N^0 depends on interfacial attraction, hydrophobic attraction and ionic head group repulsion. If this factor can be determined, average N of the solution can be calculated. As differentiating eq. (1) with N , we can check that if μ_N^0 is constant on N , smaller aggregation numbers are preferred over larger ones⁴⁰.

To find the geometry of the assembled amphiphilicities, many geometric factors must be employed. Assembled geometries are constrained by the amphiphile's molecular structure and dimensions, and this constraint called 'packing constraint'. On the outer layer of lipid membrane, packing constraint equation for sphere is⁴⁰

$$\frac{v}{a} = l \left(l - \frac{l}{R} + \frac{l^2}{3R^2} \right) \quad (2)$$

where v (m^3) is the volume of the hydrocarbon chain, a (m^2) is the effective surface area of each ionic head, R (m) is the sphere's radius and l (m) is the amphiphilic molecule's length. The parameters, v and a are assumed to be constant as material properties; and l is variable, but has critical extension limit l_c . Eq. (2) can be derived easily calculating volume and outer area of lipid shell having thickness of l and outer radius of R . When $R = l$, the spherical micelle case, eq. (2) is reduced to $l = 3v/a$. Because $l_c \geq l$, spherical micelles must satisfy the condition $l_c \geq 3v/a$. This means that lipids having $l < 3v/a$ cannot form spherical micelles. By similar derivation shown above, the cylinder micelle's constraints is $l_c \geq 2v/a$. Especially in biological components, phospholipids have two or more hydrocarbon chains. With given v , double-chained lipids have shorter l_c than single-chained lipids, approximately half. Because of this insufficient stretch of the carbon chain, these phospholipids cannot form fully-filled micelles with given v and a , and instead form a bilayer. Due to reason, a bilayer formation is preferred over micelle formation for the case of cells and exosomes dispersed in aqueous solution. Therefore, from eq. (1) and (2), phospholipids separated from cells tend to spontaneously form spherical vesicles to reduce thermodynamical energy and to satisfy geometrical constriction.

To generate small vesicles from cells by exploiting self-assembly, some forces should be induced on bigger forms of vesicles, cells (here, we use murine ES cells as the larger ones) to cut the bilayer membrane. To impose shear stress on cells, we forced them through microchannels that were fabricated using conventional soft-lithography (Figure 1a). The material of the microchannels was polydimethylsiloxane (PDMS) with contact angle (CA) $\sim 27^\circ$ after oxygen plasma treatment. The PDMS was bonded on a pyrex glass substrate. Due to the amphiphilic property of lipid molecules which directly contact the fabricated microchannel wall, the wall of the microchannel induces a shear force on the plasma membrane that can determine the behavior during vesicle shedding, depending on the surface property of the microchannel.

To observe whether cells subjected to shear can shed vesicles,

high speed CCD images (15000 frames per second) were taken as cells flowed through a microchannel (width 3 μm , height 5 μm)

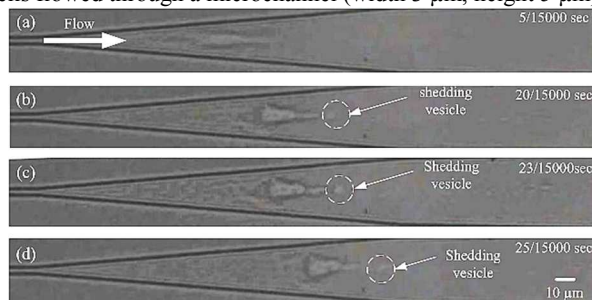


Figure 2. For imaging, a PDMS single microchannel (Width 3 μm , height 5 μm) was fabricated on a glass substrate. Images were obtained by a high speed CCD camera (15000 frames per second) when cells were extruded through a single hydrophilic microchannel. Cells were deformed through the microchannel. Expanding at the outlet of a microchannel, cells began shedding vesicles.

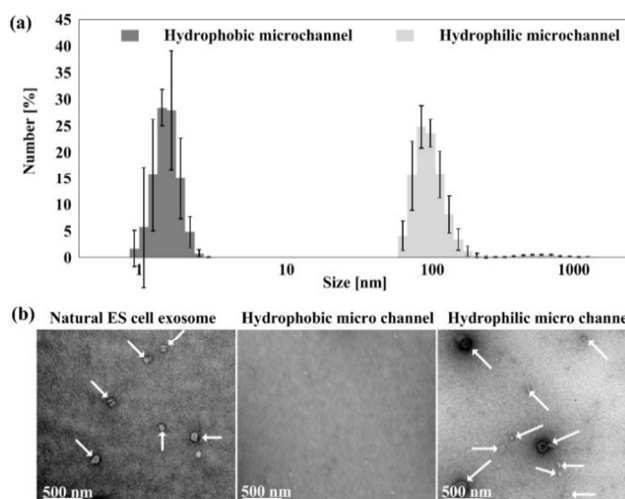


Figure 3. ES cells were extruded through microchannels with hydrophobic or hydrophilic surface. (a) DLS data of the samples after separation using an ultracentrifuge: in the samples from the hydrophilic microchannel, nano-size particles of diameter 60~120 nm were found, but in the samples from the hydrophobic channel, nano-size vesicles were not detected beyond the background signal of the buffer solution (less than 10 nm). (b) TEM image of cell-secreted exosomes and the samples. White arrows: exosomes and nanovesicles. Black or gray lines: membrane structures. Many nanovesicles in the sample from the hydrophilic microchannel having a membrane structure were observed, but no nanoparticles were observed in the sample from the hydrophobic microchannel. The morphologies of nanovesicles in the sample from the hydrophilic microchannel were similar those of to cell-secreted exosomes.

at 6.5 $\mu\text{L}/\text{min}$, which was equivalent to 43.3 m/s. An ES cell was squeezed passing through the microchannel, and shed nanoparticles at its outlet (Figure 2). Although, due to the resolution limit of optical microscopy, smaller vesicles than those shown in Figure 2 could not be observed well. These observations showed that when a cell was constricted through the microchannel the plasma membrane elongated due to resistant shear force on the surface of the microchannel. The elongated lipid bilayer was not stable thermodynamically, and eventually formed small nanoparticles.

To assess the effects of surface properties on nanoparticle formation, different device with 37 microchannels in parallel

(width 5 μm , height 10 μm , length 200 μm) were prepared with hydrophilic (CA=27°) or PTFE-coated hydrophobic surface (CA = 115°), as described in the experimental section. The flow velocity both in the hydrophilic and hydrophobic microchannels was set as 6.5 $\mu\text{L}/\text{min}$, equivalent to 0.058 m/s. The resultant transit time for which the fluid is in the microchannels was 3.45 ms. The extruded samples were collected. The samples from the hydrophilic microchannels contained fewer ES cells and more debris torn off from ES cells, whereas the samples from the hydrophobic microchannels contained more ES cells and less debris. In both hydrophilic and hydrophobic microchannels, it was hard to recognize the existing ES cells due to severe morphological damage. The ES cells in the samples were identified with trypan blue staining, and most of them were damaged in their plasma membrane by showing positive trypan blue staining. If there nanoparticles in the form of vesicles are generated, the debris are supposed to contain the nanoparticles. For analysis of the debris, the collected samples were pre-cleaned to eliminate the ES cells in the samples. Then, by using the method similar as the exosome-separation described in materials and methods, expected nanoparticles in the form of vesicles with lipid bilayer membranes were separated from the debris⁴. The sizes of separated nanoparticles were determined by dynamic laser scattering (DLS) and transmission electron microscopy (TEM). Although the sample from the hydrophobic microchannels showed a peak around several nm which accounts for background noise from ions in buffer solution, there was no peak corresponding the nanoparticles of ~ 100 nm in diameter (Figure 3a), and the TEM image also revealed no nanoparticles of ~ 100 nm in diameter (Figure 3b). In contrast, many nanoparticles of ~ 100 nm in diameter were observed as products of the hydrophilic microchannel (Figure 3a), and TEM images showed nanoparticles that had a membrane structure (Figure 3b); DLS determined that they were 60–120 nm in diameter, similar to the diameter of exosomes, and had zeta potential of -14.54 ± 1.31 mV, comparable to that of exosomes. Based on TEM images and zeta potential data, particles in the extruded sample were expected to have a lipid bilayer structure. As physical characteristics of these nanoparticles, such as morphology size and surface, were comparable to those of cell-secreted exosomes. We call these particles ‘nanovesicles’.

According to the results, the generation of nanovesicles highly depends on the surface friction of microchannels. On the hydrophilic surface, tightly constricted plasma membrane in the microchannel temporarily undergoes friction force imposed from the surface in the microchannels, and stretches in the flow direction. If the strain of the stretched membrane reaches a limit, the plasma membrane is torn into fragments (Figure 2). However, the hydrophobic wall coated with PTFE causes less friction to the cells due to low adhesiveness to biological materials. Additionally, high hydrophobicity of PTFE possibly provides non-zero surface flow velocity from slip flow condition. As a result of the combined effects, the cell slips with less friction on the surface in the microchannels, and less debris and fewer fragments of plasma membrane were generated in the hydrophobic microchannels. Even with the fewer fragments, strong hydrophobic interaction between the surface and hydrophobic carbon chains in phospholipids may disturb the

orientation of the phospholipids, not to assemble properly.

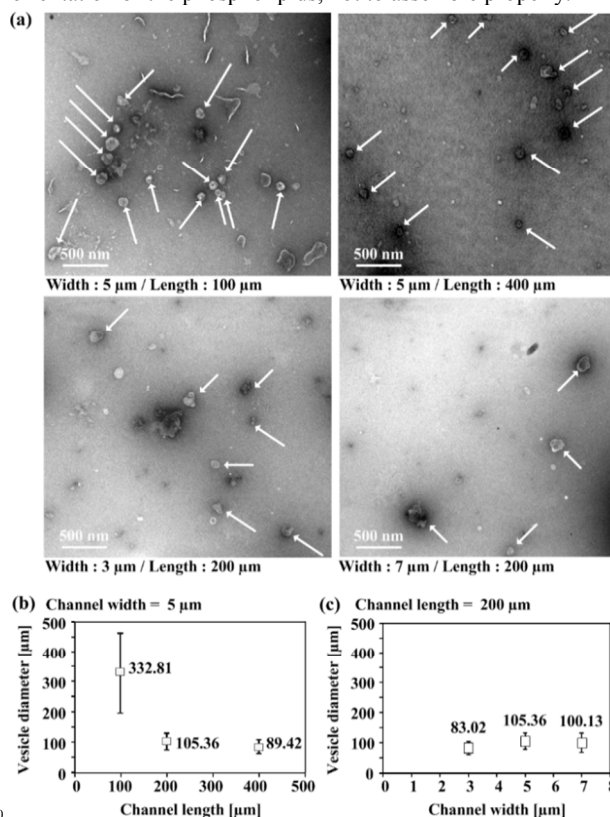


Figure 4. (a) TEM image of nanovesicles from microchannels having different length and width. Morphologies of the nanovesicle from different dimensions showed similar with closed lipid bilayers. (b) Nanovesicle sizes extruded from microchannels of three lengths (100, 200, and 400 μm) with a fixed width of 5 μm ; flow rate: 6.5 $\mu\text{L}/\text{min}$. (c) Sizes of nanovesicles extruded from microchannels with a fixed length of 200 μm , but widths of 3, 5 and 7 μm ; flow rate: 6.5 $\mu\text{L}/\text{min}$.

Size dependency on microchannel geometry

The size of nanovesicles can be varied by the degree of net force unbalancing, which can in turn be controlled by changing the microchannel's geometry, cross section area and length. As the microchannel geometry is altered, the shear force generated on cells during extrusion changes and causes nanovesicles to have different characteristics. For this experiment, the channel height was set as 10 μm . Different widths of microchannels were tested. For the microchannels with 1 μm in width, the microchannels were clogged by cells and were not able to provide meaningful data. In contrast, for the microchannels with 10 μm width, no nanovesicles were generated at all. Therefore, the range of the width of microchannels was selected from 3 μm to 7 μm .

As for volume flow rate, with volume flow rates higher than 10 $\mu\text{L}/\text{min}$, the PDMS microchannels were able to sustain the pressure built in the microchannel. In contrast to high volume flow rates, low volume flow rates required long period for extrusion a given number of the cells, which caused cell aggregation in the syringe. After trials, a flow rate of 6.5 $\mu\text{L}/\text{min}$ was chosen and the cells were extruded at the flow rate. The morphologies of nanovesicles for every case were also identified by TEM (Figure 4a); all had a closed shape after the separation process described above. The sizes of nanovesicles were quantitatively determined using DLS: the largest was generated at

the shortest microchannel length of 100 μm (transit time = 1.72 ms) but had a large variation; the mean diameter decreased abruptly at microchannel length of 200 μm (transit time = 3.45 ms), and finally converged ~ 80 nm at microchannel length of 400 μm (transit time = 6.82 ms) (Figure 4b). However, when channel width was adjusted with a fixed channel length of 200 μm , the change in mean diameters was not significant (Figure 4c). As the channel length increased, only the mean diameter of nanovesicles and their variation in size decreased. Although the main geometrical parameter to control the size of nanovesicles is the channel length; the transit time for which the friction is induced, the size of the nanovesicles with a stable structure depends on the shape of amphiphilics that comprise the nanovesicles, as described in eq. (2)

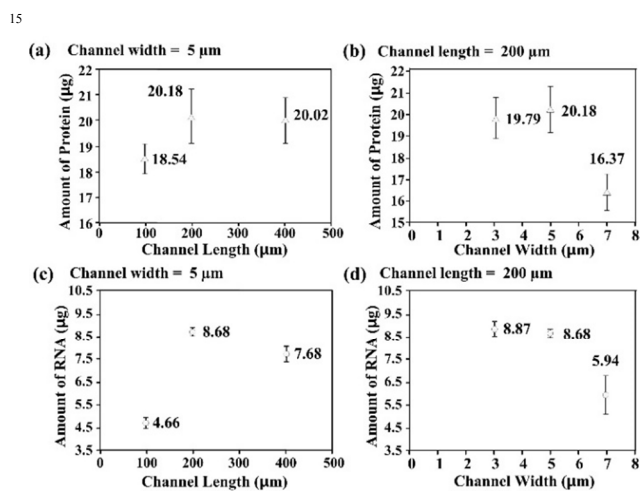


Figure 5. Protein and RNA amount after extrusion through microchannels. (a), (c) Protein and RNA amount extruded from microchannels of three lengths (100, 200, and 400 μm) with a fixed width of 5 μm ; flow rate 6.5 $\mu\text{L}/\text{min}$. (b), (d) Protein and RNA amount extruded from microchannels with a fixed length of 200 μm , but widths of 3, 5 and 7 μm ; flow rate: 6.5 $\mu\text{L}/\text{min}$.

Efficiency of generation

Similar to quantification of exosomes, these amounts of proteins and RNAs are proportional to the quantity of generated nanovesicles^{41, 42}. For the microchannel width of 5 μm , larger amount of the total proteins and RNAs in the nanovesicles were detected at the microchannel length of 200 μm (transit time=3.45 ms) than at the microchannel of 100 μm (1.72 ms). However, when the microchannel length was 400 μm (transit=6.89 ms), the amount of the total proteins and RNAs in the nanovesicles was similar to when microchannel was 200 μm (Figure 5a, c). To investigate the effect of the channel width on the total amount of proteins and RNAs in the nanovesicles, the microchannel length was fixed 200 μm , and the microchannel width was changed from 3 μm to 7 μm . The total amount of proteins and RNAs slightly increased as the microchannel width increased for 3 and 5 μm . However, for the microchannel width of 7 μm which is larger than the diameter of an ES cell, the total amount of proteins and RNAs decreased dramatically (Figure 5b, d). From these results, the proper stress or friction from the surface of the microchannel is important for fabrication of the nanovesicles. Additionally, similar as the size of nanovesicles, the main parameter to decide the amount of generated nanovesicles is also the transit time for which friction from the surface of the microchannel is applied.

Among various combinations of microchannel width and length, a combination with 200 μm length and 5 μm width was chosen for further experiments, because this combination provided nanovesicles with diameter ~ 100 nm, which is similar to that of cell-secreted exosomes. At this condition, the amount of nanovesicles was assessed by comparing the total amounts of proteins and RNAs to those from the origin ES cells and nanovesicles from an equivalent number of ES cells (Figure 6). The measured total amount of RNAs and proteins indicates that about one-fifth of the ES cells from which the nanovesicles generated. This small proportion occurred partially because many cells clogged at the entrance of the microchannels and adhered to the inside of the microchannel.

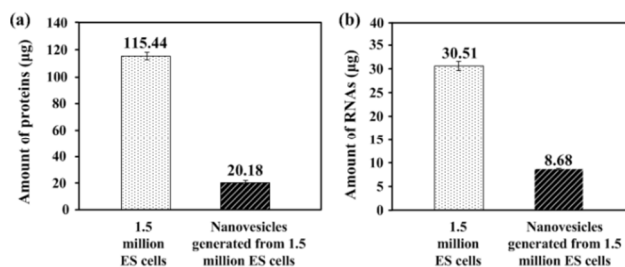


Figure 6. (a) Total protein amount and (b) total RNA amount for 1.5×10^6 original ES cells and nanovesicles generated by 1.5×10^6 ES cells. Protein was measured with Bradford assay. Proteins and RNA content of nanovesicles were $\sim 1/5$ of the amounts contained in the original cells.

Comparison with exosomes

Qualitative comparisons among origin ES cells, exosomes and nanovesicles from ES cells were performed. For the reason that the nanovesicles are generated directly from cells by extrusion, they are expected to be made up of cellular components such as plasma membrane, membrane proteins, intracellular proteins and RNAs. The presence of these components was confirmed by western blot, reverse transcription-PCR and RNA size analysis using BioanalyzerTM. Before these analyses, pre-cleaning was conducted to remove unbroken cells from the extruded sample. The western blot analysis used ICAM-1, Nanog and Beta-actin as representative markers. Nanog and Beta-actin are intracellular proteins in ES cells. All of these proteins were found in the samples from the ES cells and nanovesicles (Figure 7a); i.e., the nanovesicles have membrane proteins and contain intracellular proteins of the original cells in their lipid bilayer structure. This means that the nanovesicles are expected to contain many other proteins and intracellular materials of the original cells, much like cell-secreted exosomes. Additionally, ICAM-1 is a plasma membrane protein which is also expressed in ES cells^{40, 43}, suggesting that the separated nanovesicles contains intact plasma membrane.

The reverse transcription-PCR used Oct 3/4, Nanog and Beta-actin, typical mRNA in ES cells. All of them were also found in the ES cells, exosomes and nanovesicles (Figure 7b); this result means that the nanovesicles contain mRNAs in addition to proteins. The quality of the RNA was analysed by using BioanalyzerTM; tRNA, rRNA and microRNA were found in the ES cells, exosomes and nanovesicles, although the intensities varied depending on the samples (Figure 7c). However, RNA

profiles for ES cells and the nanovesicles are very similar; this suggests that the generated nanovesicles contain similar encapsulated contents as cells, indicating that they could be used as RNA-deliverable carriers.

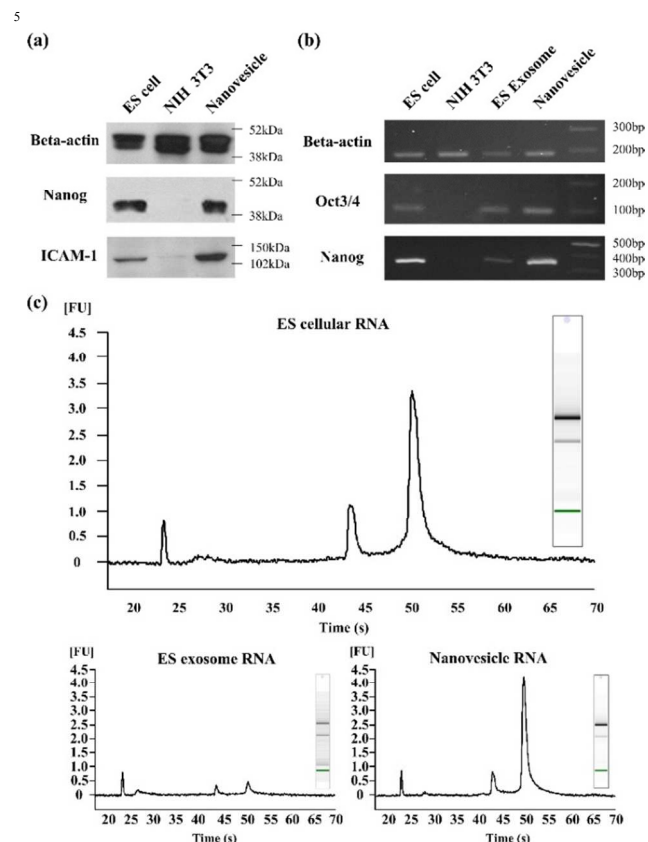


Figure 7. (a) Western blotting ES cell protein Nanog and ICAM-1 (b) reverse transcription-PCR for 10^6 original ES cells, NIH-3T3 fibroblasts, exosomes from ES cells and nanovesicles generated by 10^6 ES cells (c) RNA profiles from BioanalyzerTM for ES cells, exosomes and nanovesicles generated by 10^6 ES cells. Small non-coding RNA (25–30 sec), mRNA (25–50 sec), rRNA (43 and 52 sec) were detected in all cases.

Cellular uptake and delivery

Some studies have assumed that the amount of vesicle uptake is dependent on the chemical and physical properties of vesicles^{43–45}. To evaluate the delivery ability of the nanovesicles, cytosols of ES cells were stained with cell tracker as described above. Then, nanovesicles of ~100 nm diameter were generated by extruding the cytosol-stained ES cells through the microchannels with a width of 5 μm and length of 200 μm , and the type of lipid membrane and the concentration of membrane proteins, such as ICAM-1 in nanovesicles were supposed the same as those of original cells. The nanovesicles were treated to NIH-3T3 fibroblasts, and the amounts of uptaken nanovesicles from ES cells by NIH-3T3 fibroblasts were characterized using both a confocal microscope and fluorescence-activated cell sorting (FACS), because FACS cannot distinguish the real uptake from the attachment of nanovesicles to the plasma membrane. Confocal images were collected at various times after treatment of 10 $\mu\text{g}/\text{ml}$ nanovesicles which contained the stained cytosol of ES cells. Nanovesicles penetrated plasma membranes

and were found inside the target fibroblasts in the confocal images (Figure 8a). FACS was used to quantify amounts of uptaken nanovesicles. More than 80 % of the nanovesicles had passed through the plasma membrane after 12 h of treatment (Figure 8b). This result from FACS agrees with the amount of uptaken nanovesicles along treatment time. The uptake of the nanovesicles is effective as exosomes.

The nanovesicles contained intracellular proteins and RNAs which came from the original cells (Figure 5–7). To compare the delivery ability of the nanovesicles and exosomes, NIH-3T3 fibroblasts were treated with the nanovesicles and exosomes every two days. At day 5 after cell seeding, RNAs of the target cells were isolated for reverse transcription-PCR (Figure 8c). Exogenous genes from ES cells treated with the nanovesicles, Oct3/4 and Nanog were detected in the isolated RNAs; this result suggests that the generated nanovesicles are able to deliver their contents successfully through the plasma membrane, similarly as exosomes.

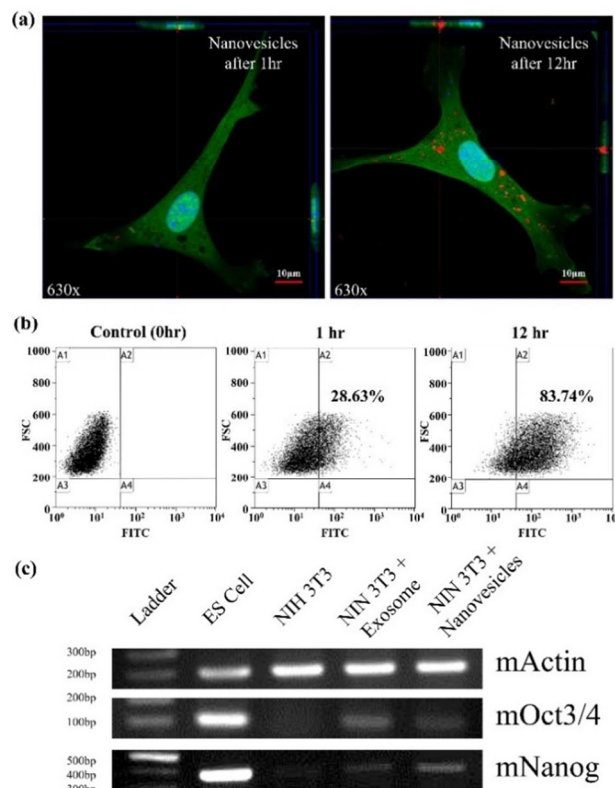


Figure 8. NIH-3T3 fibroblasts were treated with nanovesicles and exosomes from ES cells. (a) Confocal images of nanovesicle-treated NIH-3T3 fibroblasts. Images were taken 1h and 12h after treatment (red: nanovesicles; green: cytosol). (b) Flow cytometry was used to quantify nanovesicles uptaken by NIH-3T3 fibroblasts. Change of fluorescent intensity of NIH-3T3 fibroblasts along treatment time. (c) NIH-3T3 fibroblasts were treated with nanovesicles and exosomes every two days. After 5 days, RNA was isolated from target NIH-3T3 fibroblasts for PCR. Exogenous Oct 3/4 and Nanog from ES cells were detected in the isolated RNA.

Conclusions

The nanovesicles that incorporate membrane proteins were generated by extrusion of cells through a microchannel. The

shapes and contents of nanovesicles were measured and verified to be similar to those of exosomes secreted by cells; the nanovesicles had diameters of ~100 nm and had closed lipid layers. The content of the nanovesicles was identified to be intracellular proteins and RNAs. To assess the ability of these nanovesicles to deliver RNAs, target cells were treated with the nanovesicles from ES cells and the location of the nanovesicles was measured by a confocal microscope along treatment time; nanovesicles and their endogenous RNA, Oct3/4 and Nanog, were found in the target cells. The nanovesicles generated in this study showed shape and delivery ability very similar to those of exosomes, and these characteristics may be useful for many therapies and other applications.

Acknowledgements

This study was supported by grants from the National Research Foundation of Korea (NRF) funded by the Korean government (MEST; No. 2011-0028845), and partially supported by grant from the Korea Health Technology R&D Project (A120492), the KIST Institutional Program (2E23880-13-072) and the "IT consilience Creative Program" (NIPA-2013-H0203-13-1001).

References

- C. Thery, M. Ostrowski and E. Segura, *Nature Reviews Immunology*, 2009, **9**, 581-593.
- W. Perkins, S. Minchey, P. Ahl and A. Janoff, *Chemistry and Physics of Lipids*, 1993, **64**, 197-217.
- P. L. Ahl, L. Chen, W. R. Perkins, S. R. Minchey, L. T. Boni, T. F. Taraschi and A. S. Janoff, *Biochimica et Biophysica Acta (BBA)-Biomembranes*, 1994, **1195**, 237-244.
- C. Thery, L. Zitvogel and S. Amigorena, *Nature Reviews Immunology*, 2002, **2**, 569-579.
- B. Fevrier and G. Raposo, *Current opinion in cell biology*, 2004, **16**, 415-421.
- R. Juliano and D. Stamp, *Biochemical and biophysical research communications*, 1975, **63**, 651-658.
- M. L. Immordino, F. Dosio and L. Cattel, *International journal of nanomedicine*, 2006, **1**, 297.
- T. Ruysschaert, M. Germain, J. P. da Silva Gomes, D. Fournier, G. B. Sukhorukov, W. Meier and M. Winterhalter, *NanoBioscience, IEEE Transactions on*, 2004, **3**, 49-55.
- J. M. Brewer, L. Tetley, J. Richmond, F. Y. Liew and J. Alexander, *The Journal of Immunology*, 1998, **161**, 4000-4007.
- C. Ropert, *Brazilian journal of medical and biological research*, 1999, **32**.
- S. Lakhal and M. J. Wood, *Bioessays*, 2011, **33**, 737-741.
- A. Fire, S. Xu, M. K. Montgomery, S. A. Kostas, S. E. Driver and C. C. Mello, *nature*, 1998, **391**, 806-811.
- J. Zhe, A. Jagtiani, P. Dutta, J. Hu and J. Carletta, *Journal of Micromechanics and Microengineering*, 2007, **17**, 304.
- J. Moffat and D. M. Sabatini, *Nature Reviews Molecular Cell Biology*, 2006, **7**, 177-187.
- U. Fuchs, C. Damm-Welk and A. Borkhardt, *Current Molecular Medicine*, 2004, **4**, 507-517.
- L. Bonetta, *Cell*, 2009, **136**, 581-584.
- W. F. ANDERSON, *Human gene therapy*, 2002, **13**, 3-13.
- P. Lefevre, J. Attema and D. Van Bekkum, *BMC molecular biology*, 2002, **3**, 12.
- A. Sharei, J. Zoldan, A. Adamo, W. Y. Sim, N. Cho, E. Jackson, S. Mao, S. Schneider, M.-J. Han, A. Lytton-Jean, P. A. Basto, S. Jhunjunwala, J. Lee, D. A. Heller, J. W. Kang, G. C. Hartoularos, K.-S. Kim, D. G. Anderson, R. Langer and K. F. Jensen, *Proceedings of the National Academy of Sciences*, 2013.
- T. Fulmer, *SciBX: Science-Business eXchange*, 2010, **3**.
- V. Wang and W. Wu, *BioDrugs*, 2009, **23**, 15.
- K. Singha, R. Namgung and W. J. Kim, *nucleic acid therapeutics*, 2011, **21**, 133-147.
- A. R. de Fougerolles, *Human gene therapy*, 2008, **19**, 125-132.
- M. M. Lapinski, A. Castro-Forero, A. J. Greiner, R. Y. Ofoli and G. J. Blanchard, *Langmuir*, 2007, **23**, 11677-11683.
- Y. C. Tan, J. S. Fisher, A. I. Lee, V. Cristini and A. P. Lee, *Lab on a Chip*, 2004, **4**, 292-298.
- A. Utada, E. Lorenceau, D. Link, P. Kaplan, H. Stone and D. Weitz, *Science*, 2005, **308**, 537.
- K. Funakoshi, H. Suzuki and S. Takeuchi, *Journal of the American Chemical Society*, 2007, **129**, 12608-12609.
- J. C. Stachowiak, D. L. Richmond, T. H. Li, A. P. Liu, S. H. Parekh and D. A. Fletcher, *Proceedings of the National Academy of Sciences*, 2008, **105**, 4697.
- A. Pohorille and D. Deamer, *TRENDS in Biotechnology*, 2002, **20**, 123-128.
- R. T. Davies, D. Kim and J. Park, *Journal of Micromechanics and Microengineering*, 2012, **22**, 055003.
- H. Barani and M. Montazer, *Journal of liposome research*, 2008, **18**, 249-262.
- E. Atilgan and S. X. Sun, *The Journal of chemical physics*, 2007, **126**, 095102.
- J. M. Steim, M. E. Tourtellotte, J. C. Reinert, R. N. McElhaney and R. L. Rader, *Proceedings of the National Academy of Sciences*, 1969, **63**, 104.
- T. R. Brummelkamp, R. Bernards and R. Agami, *Science Signaling*, 2002, **296**, 550.
- F. Czuderna, A. Santel, M. Hinz, M. Fechtner, B. Durieux, G. Fisch, F. Leenders, W. Arnold, K. Giese and A. Klippel, *Nucleic Acids Research*, 2003, **31**, e127-e127.
- C. Théry, S. Amigorena, G. Raposo and A. Clayton, *Current Protocols in Cell Biology*, 2006, 3.22. 21-23.22. 29.
- L. Alvarez-Erviti, Y. Seow, H. Yin, C. Betts, S. Lakhal and M. J. Wood, *Nature biotechnology*, 2011, **29**, 341-345.
- A. J. Abusamra, Z. Zhong, X. Zheng, M. Li, T. E. Ichim, J. L. Chin and W.-P. Min, *Blood Cells, Molecules, and Diseases*, 2005, **35**, 169-173.
- J. N. Israelachvili, D. J. Mitchell and B. W. Ninham, *J. Chem. Soc., Faraday Trans. 2*, 1976, **72**, 1525-1568.
- J. N. Israelachvili, D. J. Mitchell and B. W. Ninham, *Biochimica et Biophysica Acta (BBA)-Biomembranes*, 1977, **470**, 185-201.
- A. Savina, M. Furlán, M. Vidal and M. I. Colombo, *Journal of Biological Chemistry*, 2003, **278**, 20083-20090.
- A. Montecalvo, A. T. Larregina, W. J. Shufesky, D. B. Stolz, M. L. Sullivan, J. M. Karlsson, C. J. Baty, G. A. Gibson, G. Erdos and Z. Wang, *Blood*, 2012, **119**, 756-766.

-
43. G. Van Meer, D. R. Voelker and G. W. Feigenson, *Nature reviews molecular cell biology*, 2008, **9**, 112-124.
44. H. Schonherr, J. M. Johnson, P. Lenz, C. W. Frank and S. G. Boxer, *Langmuir*, 2004, **20**, 11600-11606.
- 5 45. J. Kokavecz, Z. Toth, Z. L. Horvath, P. Heszler and A. Mechler, *Nanotechnology*, 2006, **17**, S173-177.

10

15